J. Neural Eng. **4** (2007) S143–S156 doi:10.1088/1741-2560/4/3/S02

An optical neural interface: *in vivo* control of rodent motor cortex with integrated fiberoptic and optogenetic technology

Alexander M Aravanis[1,5], Li-Ping Wang[1,5], Feng Zhang[1,3], Leslie A Meltzer[1], Murtaza Z Mogri[1], M Bret Schneider[2,4] and Karl Deisseroth[1,2]

[1] Department of Bioengineering, Stanford University Medical Center, Stanford, CA 94305, USA
[2] Department of Psychiatry and Behavioral Sciences, Stanford University Medical Center, Stanford, CA 94305, USA
[3] Department of Chemistry, Stanford University, Stanford, CA 94305, USA
[4] Department of Neurosurgery, Stanford University Medical Center, Stanford, CA 94305, USA

E-mail: deissero@stanford.edu

Received 8 February 2007
Accepted for publication 2 May 2007
Published 1 June 2007
Online at stacks.iop.org/JNE/4/S143

Abstract

Neural interface technology has made enormous strides in recent years but stimulating electrodes remain incapable of reliably targeting specific cell types (e.g. excitatory or inhibitory neurons) within neural tissue. This obstacle has major scientific and clinical implications. For example, there is intense debate among physicians, neuroengineers and neuroscientists regarding the relevant cell types recruited during deep brain stimulation (DBS); moreover, many debilitating side effects of DBS likely result from lack of cell-type specificity. We describe here a novel optical neural interface technology that will allow neuroengineers to optically address specific cell types *in vivo* with millisecond temporal precision. Channelrhodopsin-2 (ChR2), an algal light-activated ion channel we developed for use in mammals, can give rise to safe, light-driven stimulation of CNS neurons on a timescale of milliseconds. Because ChR2 is genetically targetable, specific populations of neurons even sparsely embedded within intact circuitry can be stimulated with high temporal precision. Here we report the first *in vivo* behavioral demonstration of a functional optical neural interface (ONI) in intact animals, involving integrated fiberoptic and optogenetic technology. We developed a solid-state laser diode system that can be pulsed with millisecond precision, outputs 20 mW of power at 473 nm, and is coupled to a lightweight, flexible multimode optical fiber, ~200 μm in diameter. To capitalize on the unique advantages of this system, we specifically targeted ChR2 to excitatory cells *in vivo* with the CaMKIIα promoter. Under these conditions, the intensity of light exiting the fiber (~380 mW mm^{-2}) was sufficient to drive excitatory neurons *in vivo* and control motor cortex function with behavioral output in intact rodents. No exogenous chemical cofactor was needed at any point, a crucial finding for *in vivo* work in large mammals. Achieving modulation of behavior with optical control of neuronal subtypes may give rise to fundamental network-level insights complementary to what electrode methodologies have taught us, and the emerging optogenetic toolkit may find application across a broad range of neuroscience, neuroengineering and clinical questions.

[5] These authors contributed equally.

1. Introduction

A common goal of physiologists, physicians and bioengineers is to elucidate the properties and control the pathologies of specific classes of excitable cells within native tissue. For example, in neuroscience, genetically targeted and temporally precise manipulation of neuronal activity would enable exploration of the causal function of individual neuron types in intact circuits. In the clinical setting, precise control over specific molecularly distinct cell types within intact tissue would drive new understanding of excitable-cell pathophysiology and almost certainly lead to development of novel treatments. Indeed, malfunctions in specific types of electrically excitable cells contribute not only to neuropsychiatric diseases such as Parkinson's disease, Alzheimer's disease, pain syndromes, epilepsy, depression and schizophrenia, but also to non-neural diseases including heart failure, muscular dystrophy and diabetes.

The temporal precision of electrode stimulation has led to powerful therapies in clinical neuroscience and to remarkable insights in basic neuroscience [1–10]. Indeed, neuromodulation of deep brain structures with surgically implanted electrodes has brought about a revolution in the treatment of movement disorders [11–14]. A similar revolution is poised to take place in psychiatry, where modulation of targeted brain structures holds great promise for the treatment of many neuropsychiatric conditions [15]. However, difficulties persist that influence the application of electrodes to behaving animals and human beings. Most importantly, extracellular electrodes have limited cellular specificity. It is generally impossible to target specific classes of neurons in heterogeneously populated tissue with extracellular electrodes, which indiscriminately activate excitatory neurons, all classes of inhibitory neurons, and fibers of passage in the stimulated area.

This problem, in addition to presenting major challenges for neuroscientists seeking to probe the role of specific cell types in behavior, is thought to contribute to the inconsistent efficacy and sometimes serious side effects seen in clinical deep brain stimulation. Stimulation-induced side effects can result from the unintended stimulation of non-targeted brain regions [16] or from the 'collateral damage' of stimulating non-therapeutic cell types within the targeted tissue. For example, DBS to the thalamus can induce parasthesias, muscular cramps, dystonia, dizziness, dysarthria, gait disturbance, balance disturbance, limb ataxia, impaired proprioception and decreased fine motor movement [17, 18]. DBS to the globus pallidus can produce confusion, depression, increased dyskinesia, gait and speech disturbances [17, 18]. DBS to the subthalamic nucleus may produce increased dyskinesia, spasm of the eyelids, confusion, memory disturbance, personality changes, mood changes, apathy, dysphonia, dysarthria and weight gain [16–20]. Because electrical spread into non-targeted regions is one cause of DBS side effects, side effects can often be reduced or eliminated by adjusting the electrical pulse parameters. Unfortunately, an improved side effect profile is frequently accomplished at the cost of decreased treatment efficacy [18]. New technologies in neural stimulation are clearly needed to deliver improved stimulation efficacy without an increased side effect profile.

Employing light to activate neurons has emerged as an attractive new concept (for review, see [21–24]). Leveraging advances in chemical biology and molecular genetics, several groups have developed novel optical techniques to control neural activity, involving optical uncaging of chemically modified neurotransmitters [25–27], chemical modification of native proteins to render them light-responsive [28, 29] or introduction of light-sensitive proteins into cells [27, 30–36]. These pioneering techniques provided different levels of temporal and spatial control of stimulation, but most required addition of special chemical chromophores to the preparation, a limitation which essentially prevented application to intact mammals.

Channelrhodopsin-2 (ChR2), an algal light-activated cation channel we have developed for use in mammals [30], can give rise to nontoxic, light-driven stimulation of CNS neurons on a timescale of milliseconds, allowing precise quantitative coupling between optical excitation and neuronal activation [22, 30–32, 37, 38]. Because ChR2 is genetically targetable, specific populations of neurons embedded within intact circuitry in principle can be stimulated with high temporal precision. We recently developed lentiviral methods to deliver ChR2 *in vivo* to adult rodents by stereotactic injection. Initial experiments in brain slices showed structurally intact neuronal somata and dendrites expressing ChR2, and upon living acute slice preparation, ChR2 exhibited the same rapid photoactivatable kinetics in intact neural tissue as we had demonstrated in culture [22]. Indeed, we could drive reliable spike trains of up to 50 Hz, and millisecond-scale spike timing precision could be maintained even in sustained high-frequency trains. While ChR2 requires the presence of all-*trans*-retinal (ATR) to function, an important consideration for applications *in vivo*, we found that endogenous ATR in the mammalian brain is sufficient for the functioning of ChR2, allowing activation of neurons *in situ* without added cofactors, in sustained yet temporally precise trains of spikes.

These experiments from acute brain slices, while demonstrating the safety and cofactor-independence of ChR2 in intact tissue, did not solve the problem of *in vivo* light delivery to intact animals, an entirely distinct bioengineering challenge. We therefore set out to develop a method of performing cell type-specific optical stimulation in an intact mammal. Development of such an optical neural interface could allow real-time modulation of complex circuits in awake, behaving animals, with an enormous range of possible applications. We targeted the rodent vibrissal motor system, a well-studied circuit [39, 40] with a validated and quantifiable assay for activation, namely deflection of the whiskers. We hypothesized that we could achieve optical control of whisker deflection by expressing ChR2 in the excitatory motor neurons of layer 5 vibrissal motor cortex. The core optical technology we developed includes a blue laser diode coupled to an optical fiber. The solid-state laser diode can be pulsed with millisecond precision, outputs 20 mW of power at 473 nm, and is coupled to a flexible stripped multimode optical fiber

~200 μm in diameter. The intensity of light exiting the fiber end is ~380 mW mm^{-2}, sufficient to excite ChR2+ neurons within millimeters of the fiber end even accounting for the significant attenuation seen in intact tissue. Achieving modulation of behavior with optical control of neuronal subtypes in this way may give rise to crucial network-level insights, and find application across a broad range of neuroscience and neuroengineering questions.

2. Materials and methods

2.1. Lentivirus production and transduction

Lentiviral vectors carrying the mammalianized-codon ChR2-mCherry fusion gene under control of the CaMKIIα promoter, to target excitatory cortical neurons, were constructed using standard cloning techniques. Briefly, mCherry (courtesy of Dr Roger Tsien at UCSD), with the start codon removed, was fused in-frame to the carboxyl terminus of ChR2 via a Not*I* linker. The ChR2-mCherry fusion gene was then PCR amplified and inserted into a lentiviral plasmid carrying a 1.3 kb fragment of the CaMKIIα promoter (courtesy of Dr Pavel Osten at the Max-Planck-Institut Für Medizinische Forschung) via the Age*I* and Eco*RI* restriction sites. High titer lentivirus ($>10^9$ pfu mL^{-1}) was then produced via calcium-phosphate co-transfection of 293FT cells (Invitrogen) with the lentiviral vector, pCMVΔR8.74 and pMD2.G [22]. 24 h post-transfection, 293FT cells were switched to serum-free medium (ULTRACulture; Cambrex) containing 5 mM sodium butyrate; the supernatant was collected 16 h later and concentrated by ultracentrifugation at 50 000 $\times$ *g* with 20% sucrose cushion. The resulting viral pellet was resuspended in phosphate buffered saline at 1/1000th of the original volume.

2.2. Stereotactic viral delivery and preparation of acute brain slices

Rats (male Wistars, 250–350 g) and mice (female C57/BL6, 25–30 g) were the subjects of these experiments. Animal husbandry and all aspects of experimental manipulation of our animals were in strict accord with guidelines from the National Institute of Health and have been approved by members of the Stanford Institutional Animal Care and Use Committee. Rats were anaesthetized by i.p. injection (90 mg ketamine and 5 mg xylazine per kg of rat body weight). Concentrated lentivirus solution was stereotactically injected into the rat motor cortex (anteroposterior = -1.5 mm from bregma; lateral = 1.5 mm; ventral = 1.5 mm). For electrophysiological experiments, 2 weeks post-injection, 250 μm cortical slices were prepared in ice-cold cutting buffer (64 mM NaCl, 25 mM $NaHCO_3$, 10 mM glucose, 120 mM sucrose, 2.5 mM KCl, 1.25 mM NaH_2PO_4, 0.5 mM $CaCl_2$ and 7 mM $MgCl_2$, equilibrated with 95% O_2/5% CO_2) using a vibratome (VT 1000 S; Leica). After a recovery period of 30 min in cutting buffer at 32–35 °C, slices were gently removed to a recording chamber mounted on an upright microscope (DM LFSA, Leica) and continuously perfused at a rate of 3–5 ml min^{-1} with carbonated ACSF (124 mM NaCl, 3 mM KCl, 26 mM $NaHCO_3$, 1.25 mM NaH_2PO_4, 2.4 mM $CaCl_2$, 1.3 mM MgCl2, 10 mM glucose), ventilated with 95% O_2/5% CO_2.

2.3. Cellular identification, electrophysiology and optical stimulation methodology

Motor cortex slices were visualized by standard transmission optics on an upright fluorescence microscope (DM LFSA; Leica) with a 20×, 0.5 NA water immersion objective. mCherry expressing cells located about 10–30 μm below the surface of the slice were visualized with a TXRED filter set (TXRED 4040B, exciter 562 nm, dichroic 530–585 nm, emitter 624 nm; Semrock). Images were recorded with a cooled CCD camera (Retiga Exi; Qimaging). Electrophysiological recordings in neurons were performed as previously described [30]. Briefly, membrane currents were measured with the patch-clamp technique in the whole cell voltage-clamp configuration using Axon Multiclamp 700B (Axon Instruments) amplifiers. Pipette solution consisted of (in mM) 97 potassium gluconate, 38 KCl, 6 NaCl, 0.35 sodium ATP, 4 magnesium ATP, 0.35 EGTA, 7 phosphocreatine and 20 HEPES (pH 7.25 with KOH). Pipette resistance was 4–8 MΩ. To obtain an estimate of the resting potential, we noted the membrane potential at the time of establishing the whole cell configuration. pClamp 9 software (Axon Instruments) was used to record all data. For ChR2 activation, blue light pulses were generated using the DG-4 high-speed optical switch with a 300 W xenon lamp (Sutter Instruments) and a GFP filter set (excitation filter HQ470/40×, dichroic Q495LP; Chroma). The light pulses were delivered to the slice through a 20× objective lens (NA 0.5; Leica) yielding a blue light intensity of 10 mW mm^{-2}, measured with a power meter (1815-C; Newport). Electrophysiological experiments were performed at room temperature (22–24 °C).

2.4. Measurement of light transmission through rodent cortex

Light transmission measurements were conducted with acute brain slices from a 300 g rat and a 30 g mouse. Brain slices of thicknesses between 200 μm and 1 mm were cut in 0–4 °C sucrose solution using a vibratome (Leica; VT1000S). The brain slices were then placed in a Petri dish containing the same sucrose solution over the photodetector of a power meter (ThorLabs; S130A). The tip of a 200 μm diameter optical fiber (BFL37–200; Thorlabs) coupled to a blue diode laser (473 nm, CrystaLaser) was mounted on a micromanipulator and then positioned over the cortical tissue in the slice, normal to the slice and detector. The tip was submerged into the solution and moved to 1 mm above the tissue surface. Blue light from the diode laser was delivered to the tissue via the optical fiber and a measurement of the total light power was recorded from the power meter. The fiber tip was then translated horizontally, so that a blank measurement without tissue present could be taken. For each slice, one measurement was taken from each hemisphere. For each tissue thickness value, two different slices were cut and measured. Transmission fraction was calculated as the power with tissue present divided by the power with no tissue present. Transmission of light through the brain slices was modeled using the Kubelka–Munk model for diffuse scattering media,

$$T = \frac{1}{Sz + 1},$$

where T is transmission fraction, S is the scatter coefficient per unit thickness and z is the thickness of the sample [41]. The model assumes that the sample is a planar, homogeneous, ideal diffuser, which is illuminated from one side with diffuse monochromatic light. The model further assumes that reflection and absorption are constant over the thickness of the sample. To further simplify the model, it was also assumed that no absorption occurs. This assumption is based on previous *in vivo* and *in vitro* data showing that in mammalian brain tissue, transmission loss from scattering is much greater than loss from absorption for wavelengths ranging from 400 to 900 nm [42, 43]. Best fit values for S were 11.2 mm^{-1} for mouse and 10.3 mm^{-1} for rat. The complete relationship of light intensity to tissue penetration distance was estimated by taking the product of the measured transmission fraction (remaining light not scattered or absorbed) and the calculated fractional decrease in intensity due to the conical geometry of emitted light at a given distance in the absence of tissue scattering and absorption. The half-angle of divergence θ_{div} for a multimode optical fiber is

$$\theta_{div} = \sin^{-1}\left(\frac{NA_{fib}}{n_{tis}}\right),$$

where n_{tis} is the index of refraction of gray matter (1.36, [41]) and NA_{fib} (0.37) is the numerical aperture of the optical fiber. Assuming conservation of energy, the geometric decrease in intensity with distance from the fiber end z was calculated,

$$\frac{I(z)}{I(z=0)} = \frac{\rho^2}{(z+\rho)^2}, \quad \text{(geometric component only)}$$

where

$$\rho = r\sqrt{\left(\frac{n}{NA}\right)^2 - 1}$$

and r is the radius of the optical fiber. The complete expression for intensity taking into account both the scattering and geometric losses is

$$\frac{I(z)}{I(z=0)} = \frac{\rho^2}{(Sz+1)(z+\rho)^2}.$$

2.5. Implantation of optical neural interface and viral delivery

Surgeries were performed under aseptic conditions. For anesthesia, ketamine (90 mg kg^{-1} of rat body weight; 16 mg kg^{-1} of mouse body weight) and xylazine (5 mg kg^{-1} of rat body weight; 5 mg kg^{-1} of mouse body weight) cocktail was injected i.p. The level of anesthesia was carefully monitored and maintenance doses of anesthesia were given as needed. Fur was sheared from the top of the animal's head and the head was placed in a stereotactic positioning rig. A midline scalp incision was made and a 1 mm diameter craniotomy was drilled: rat: anteroposterior = −1.5 mm from bregma, lateral = 1.5 mm; mouse: anteroposterior = −1 mm from bregma, lateral = 1 mm. A fiber guide (C313G; Plastics1) was then inserted through the craniotomy to a depth of 1.5 mm in the rat and 1.3 mm in the mouse. Three skull screws (00–96 × 3/32; Plastics1) were placed in the skull surrounding the fiber guide pedestal, and cranioplastic cement (Ortho-Jet; Lang Dental) was used to anchor the fiber guide system to the skull screws. After 30 min, the free edge of the scalp was brought to the base of the cranioplastic cement using sutures (3–0 silk; Ethicon) and tissue adhesive (Vetbond; 3M). A 2 μL aliquot of concentrated lentiviruses in solution (described above) was slowly injected through the fiber guide using an internal cannula (C313I; Plastics1) over 5 min. After waiting 10 more min for diffusion of the lentivirus, the internal cannula was withdrawn, and a dummy cannula (C313G; Plastics1) was inserted to keep the fiber guide patent.

2.6. Whisker deflection assay

Animals were lightly anesthetized with a 50% dose of the ketamine and xylazine cocktail described above. For these experiments we kept animals in only a lightly sedated state, where whisker deflections spontaneously occurred, as heavier sedation abolished both spontaneous and evoked responses and with no sedation the spontaneous activity was so vigorous it obscured any evoked activity. The method for whisker deflection measurement was based on previous work [44]. Briefly, whiskers contralateral to the fiber guide implantation were trimmed to 1 cm in length, and a 1 mg rare-earth magnetic particle (neodymium-iron-boron; Magcraft) was attached to the C2 vibrissa. The head was then placed in a stereotactic rig with minimal pressure applied. To measure whisker movement, a magnetoresistive sensor (HMC1001; Honeywell) was mounted on a micromanipulator and moved near the magnetic particle. The signal was amplified (410; Brownlee) and recorded to a computer. Signals were high-pass filtered at 10 Hz to remove low-frequency drift arising from head movement and breathing. Stimulation of ChR2+ neurons was accomplished using a multimode optical fiber (NA 0.37) with a 200 μm silica core (BFL37–200; Thorlabs) coupled to a 473 nm diode pumped laser (20 mW output power uncoupled; CrystaLaser). The measured light intensity emanating from the fiber was 380 mW mm^{-2}. The distal end of the fiber was polished and the jacket was stripped; the fiber was inserted into the fiber guide and advanced until flush with the fiber guide end. The animal was then allowed to habituate to the setup. Experiments were initiated once spontaneous whisker twitches greater than 0.5° were present. During an experimental sweep, 30 s of pre-stimulus data, 20 s of intra-stimulus data (20 s pulse of blue light) and 30 s of post-stimulus data were recorded.

2.7. Immunohistochemistry

Three weeks after photostimulation, a subset of mice were anesthetized with ketamine/xylazine and sacrificed by transcardial perfusion with ice cold 4% paraformaldehyde (PFA) in phosphate buffered saline (PBS). Extracted brains were incubated overnight in 4% PFA/PBS and for 48 h in 30% sucrose/PBS. 40 μm sections were cut on a Leica freezing microtome and stored in cryoprotectant at 4 °C. For immunostaining, free-floating sections were rinsed twice in Tris-buffered saline (TBS, pH 7.5) and blocked for 30 minutes in TBS++ (TBS/0.3% Triton X-100/3% normal donkey serum (NDS)). Both primary and secondary antibody incubations were conducted overnight at 4 °C in TBS++ with NDS reduced to 1%; sections were washed repeatedly in TBS after each

antibody incubation. Antibodies used were rabbit anti-dsRed (1:500, Clontech), mouse anti-CaMKIIα (1:200; Chemicon), mouse anti-GAD67 (1:500, Chemicon), Cy3 donkey anti-rabbit (1:1000; Jackson ImmunoResearch) and FITC donkey anti-mouse (1:1000, Jackson). Stained sections were mounted under PVA-Dabco (Sigma). Confocal images were acquired on a Leica TCS SP2 microscope. Statistics on cell phenotype were determined by counting mCherry positive cells in thin sections within the targeted deep cortical layers >50 μm from the optical fiber tract for optimal immunohistochemistry. In four 40 nm thick sections, 19 of 20 mCherry positive cells were also positive for CaMKIIα. In three other 40 nm thick sections, 0 of 30 mCherry positive cells were also positive for GAD67.

3. Results

3.1. Optical neural interface design

Beginning with our initial adaptation of the algal ion channel ChR2 to mammalian neurons [30], a growing number of investigators now have demonstrated robust photoactivation of ChR2-expressing (ChR2+) neurons in neuronal cultures and brain slice [22, 30–33, 37, 38]. However, a method for *in vivo* activation of mammalian behavior has yet to be demonstrated. There are a number of technical challenges that must be overcome to accomplish *in vivo* modulation of mammalian behavior using ChR2. First, blue light (required for gating ChR2) is highly scattered in brain tissue [42, 43] placing limits on the volume of tissue in which the intensity required for spiking is achieved (intensity $\geqslant 1$ mW mm^{-2} according to *in vitro* work by our lab and others [22, 30–33, 37, 38]). For photostimulation of the superficial layers of cortex, and perhaps deeper into cortex using two-photon systems, surface imaging systems based on microscope objectives could be adapted to deliver light through window craniotomies [45]. However, for deeper brain structures and for awake behaving animals (the ultimate goal for neural interface development) these bulky systems are not suitable. Another challenge is that the illumination must correctly target the region that has been rendered photosensitive with ChR2. In practice, this region where ChR2 has been expressed is often <1 mm^3 in volume, depending on the type of viral vector, the method of injection and the quantity of viral particles injected [22].

We developed a novel optical neural interface (ONI) to address these problems and functionally activate ChR2 in an intact animal. The interface consisted of an optical fiber guide stereotactically mounted to the skull with an optical fiber inserted through the guide (figure 1(a)). The fiber guide is composed of a cannula embedded in a mounting pedestal. The system serves two purposes. First, for viral transduction of neurons, the fiber guide serves as an injection cannula to deliver the viral vector to the motor cortex. Then following expression of ChR2, the cannula is used to guide the optical fiber to the correct location, positioning the tip so the light beam is registered with the ChR2+ neurons. By using the same cannula for viral delivery and positioning of the optical fiber, we achieve confidence that the light beam is correctly

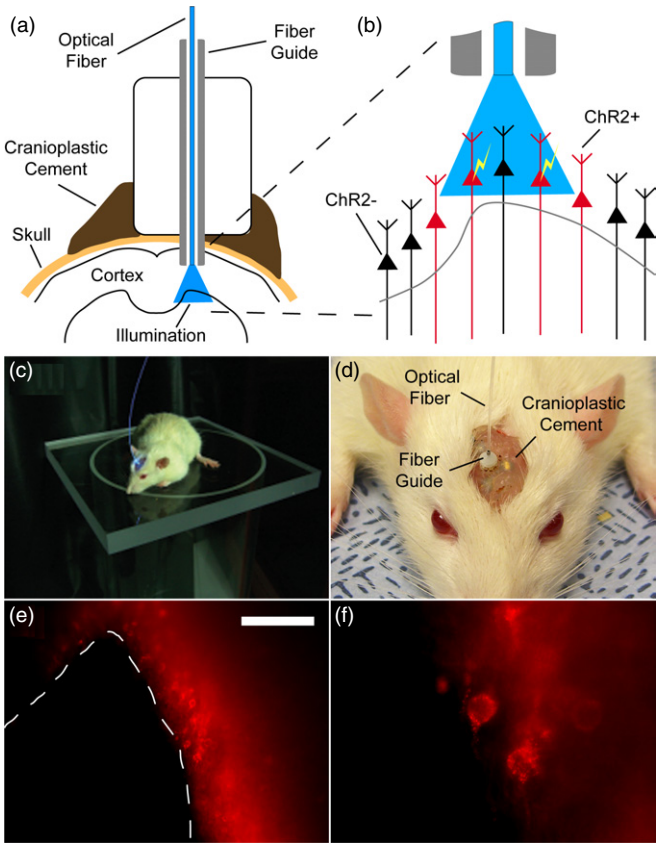

Figure 1. Overview of the optical neural interface. (a) Schematic of optical neural interface mounted on a rat skull, showing optical fiber guide, optical fiber inserted and blue light transmitted to the cortex. 2 weeks prior to testing, lentivirus carrying the ChR2 gene fused to mCherry under control of the CaMKIIα promoter was injected through the fiber guide. (b) Close-up schematic of the stimulated region. The optical fiber tip is flush with the fiber guide and blue light is illuminating the deeper layers of motor cortex. Only glutamatergic pyramidal neurons that are *both* in the cone of illumination and genetically ChR2+ will be activated to fire action potentials. (c) Rat with optical neural interface implanted; blue light is transmitted to target neurons via the optical fiber. (d) Close-up view of the optical neural interface showing fiber guide attached with translucent cranioplastic cement. Note that no scalp or bone is exposed. (e) Low-power mCherry fluorescence image of acute brain slice showing rat motor cortex after removal of optical neural interface. The edge of the tissue displaced by the optical fiber is demarcated with a dashed line. Numerous mCherry+ neurons around the distal end of the fiber guide are present. Scale bar is 250 μm. (f) High-power image of mCherry+ neurons showing membrane-localized fluorescence characteristic of ChR2-mCherry fusion protein expression.

registered to the ChR2+ neurons (figure 1(b)). Figure 1(c) shows a rat with the ONI implanted and blue light transmitted to the ChR2+ neurons. Figure 1(d) is a close-up of the head showing the fiber guide attached with cranioplastic cement and an optical fiber inserted into the guide.

To validate the utility of the fiber guide system, it was first important to verify that ChR2 could be expressed by injection of virus through the fiber guide. Acute rat brain slices (2 weeks post-injection through the fiber guide with lentivirus carrying the ChR2-mCherry fusion protein) displayed large numbers of red-fluorescent layer 4, 5 and 6 neurons in motor cortex,

revealing robust ChR2-mCherry expression (figure 1(e)). As expected, and required for the optical interface to function, the optical fiber creates a tract by displacing tissue. The fluorescent neurons were located near the edge of the tissue displaced by the optical fiber. At higher magnification, the red fluorescence appeared to be preferentially localized to the plasma membrane in these neurons (figure 1(f)), consistent with previous observations of mCherry-ChR2 expression [22]. These data suggested that the targeted expression and spatial registration functions of the cannula/fiber guide system could be suitable for implementing an optical neural interface.

3.2. Expression of channelrhodopsin-2 in vibrissal motor cortex

Before attempting intact-animal experiments, it was important to confirm that functional ChR2 could be expressed in the targeted excitatory motor neurons of layer 5 motor cortex. To test this possibility, lentivirus carrying the ChR2-mCherry fusion protein under the control of an excitatory neuron-specific CaMKIIα promoter [46, 47] was stereotactically injected into rat vibrissal motor cortex, where brain slices of the injected region made 2 weeks post-injection showed the expected significant red fluorescence (mCherry) in the deeper layers of the cortex (figures 2(a), (b)). In these same slices, we next tested whether the level of ChR2 expression in these neurons and with this promoter would be sufficient to induce the depolarizing photocurrents required for action potential generation. Indeed, whole cell recordings obtained from these ChR2+ layer 5 motor neurons in acute brain slices showed robust spiking in response to illumination with blue light (473 nm; 10 mW mm^{-2} generated by a 300 W xenon lamp and 20×, 0.5 NA objective) (figure 2(c)). In fact, the ChR2+ neurons were able to follow photostimulation trains (10 ms pulses) at 5, 10 and 20 Hz (figures 2(c), (d) and (f)). Moreover, the neurons generated an action potential for every light stimulus; figure 2(e) shows that failures were never observed even over multiple sustained trains of 10 Hz light pulses.

Having developed and validated the genetic technology required for the *in vivo* experiments, we next sought to develop and validate the optical technology. For this purpose, we evaluated a fiber-coupled diode laser for its ability to evoke photocurrent induced action potentials. Whole cell recordings were obtained from a ChR2+ layer 5 motor neuron in acute brain slices prepared as in figures 2(a)–(e), illuminated in this case not by the xenon lamp and 20× objective but by the polished end of a 200 μm multimode optical fiber. With the fiber tip placed 1 mm away from the microelectrode tip, the closest distance practically achievable for combined whole-cell patch clamp, the neuron perfectly followed a train of photostimuli at 2 Hz (figure 1(f)). As the frequency increased beyond 2 Hz, there were an increasing number of failures, where the photocurrents evoked were insufficient to depolarize the neuron to the threshold of action potential generation. Since the light intensity exiting the fiber end is quite high (∼380 mW mm^{-2}), the decrease in efficacy with fiber illumination at higher frequencies is likely due to a rapid decrease in the effective light intensity at significant distances

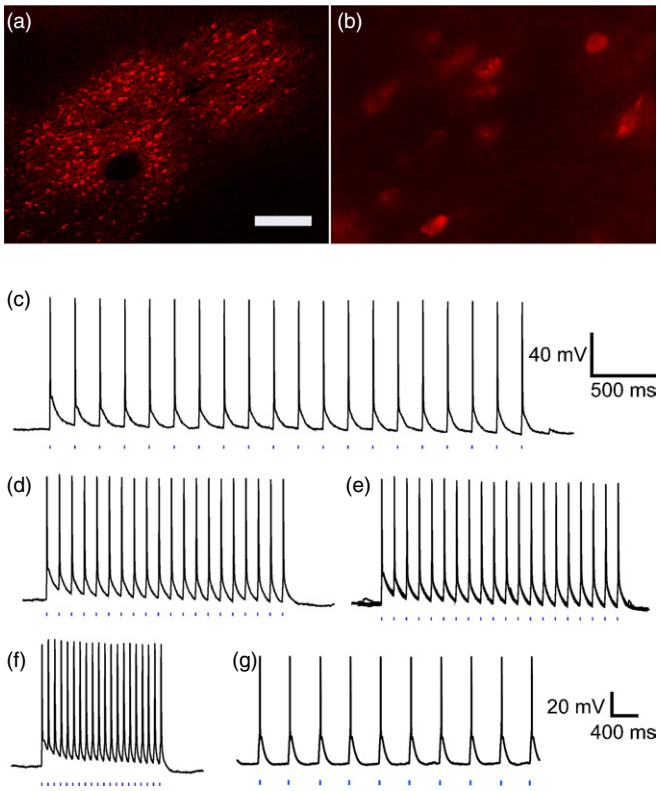

Figure 2. Functional expression of ChR2 in intact rat cortical slice. (a) Scanning confocal image of layer 4–6 pyramidal neurons in adult motor cortex expressing ChR2-mCherry in the acute slice (mCherry fluorescence visualized with 5× objective). Scale bar = 200 μm. (b) Confocal image corresponding to (a) using 20× objective. (c), (d), (f) Current clamp recordings from a layer 5 cortical pyramidal neuron in the acute adult rat slice showing action potentials evoked by 5, 10, or 20 Hz trains of light pulses (each blue dash represents a single 10 ms light flash). (e) Nine consecutive spike trains at 10 Hz (180 spikes resulted from 180 light flashes) superimposed to demonstrate the low temporal jitter, reliability and sustainability of ChR2-based photostimulation. Scale bars for (c) to (f) displayed in (c) are 40 mV and 500 ms. Light pulses were delivered via the 20× microscope objective producing a light intensity of ∼10 mW mm^{-2}. All experiments were performed without the addition of any exogenous chemical cofactor. (g) Fiber optic activation of ChR2 in acute rat cortical slice using 2 Hz trains of light pulses with 30 ms duration. Each light pulse evoked one action potential under this condition. The optical fiber was a 200 μm multimode silica-core fiber coupled to a blue-laser diode (methods). The wavelength was 473 nm and the light intensity at the fiber tip was ∼380 W mm^{-2}. The tip of the optical fiber was placed 1 mm from the patch-clamped neuron. Scale bars for (g) are 20 mV and 400 ms.

distal to the fiber tip. Presumably, ChR2+ neurons closer to the fiber than were accessible by whole-cell patch clamp received a higher light intensity and therefore followed action potential trains more reliably.

3.3. Propagation of blue light in cortical tissue

For this work, it was important to understand the physical processes and device parameters determining the volume of ChR2+ neurons that can be effectively photostimulated. This volume should correspond to the brain volume in which the light intensity achieved is greater than ∼1 mW mm^{-2}, the

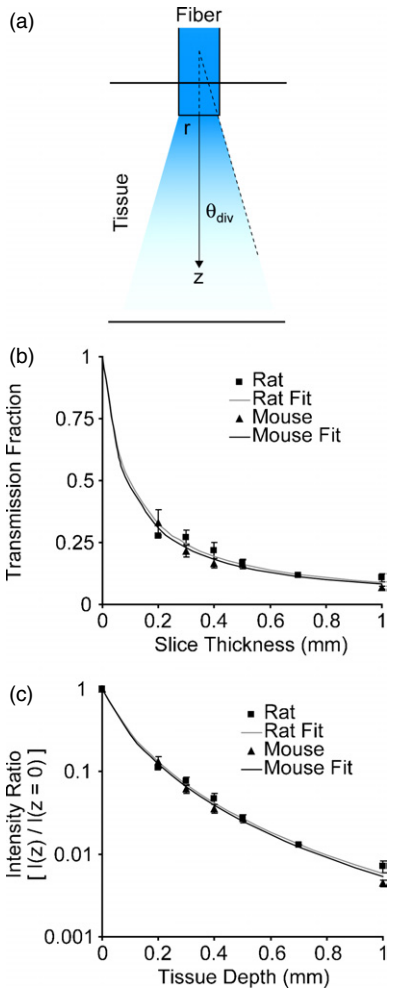

Figure 3. Blue light propagation through cortical tissue. (a) Schematic of experimental setup, showing the relationship between the optical fiber, brain tissue and attenuating light (r: optical fiber radius; z: tissue depth from fiber end; θ_{div}: the half-angle of divergence). (b) The experimentally measured total transmission fraction of 473 nm light through different thicknesses of cortical brain tissue is shown for rat ($n = 4$, 2 slices from each of two hemispheres) and mouse ($n = 4$, 2 slices from each of two hemispheres). Error bars indicate one standard deviation from the mean. The fits were produced using the Kubelka–Munk model of light transmission through diffuse scattering media (methods). (c) Calculated light intensity ratio of 473 nm light as a function of tissue depth z. The ratio represents the intensity (mW mm^{-2}) of light after transmission through a given tissue thickness divided by the intensity of the light emanating from the optical fiber tip. Calculation of intensity was based on both the experimental data and the Kubelka–Munk fits and incorporates effects of both scattering and conical spread of the beam as determined by the optical fiber's numerical aperture (methods).

minimum intensity required for generation of ChR2-evoked action potentials [22, 30–33, 37, 38]. The light intensity exiting the 200 μm diameter optical fiber tip is ∼380 mW mm^{-2}, sufficiently intense to evoke action potentials. For these experiments, the blue light used for ChR2 activation (473 nm) is near the ChR2 peak absorption wavelength [35], but brain tissue highly scatters and weakly absorbs light at this wavelength [42, 43]. Figure 3(a) shows the experimental setup. First, we directly measured the transmission fraction of total transmitted blue light as a function of distance through the rat and mouse cortical tissue (figure 3(b)). We found that after passing through 100 μm of cortical tissue, total transmitted light power was reduced by 50%, and by 90% at 1 mm (figure 3(b)). Similar results were obtained in rat and mouse tissue, and both sets of data (figure 3(b)) corresponded very well with the Kubelka–Munk model for diffuse scattering media (Methods), with best fit values for S of 11.2 mm^{-1} for mouse and 10.3 mm^{-1} for rat.

In addition to loss of light from scattering and absorption, light intensity also decreases as a result of the conical spreading of light after it exits the optical fiber. The light exiting the multimode fiber is not collimated and spreads with a conical angle of 32° determined by the numerical aperture of 0.37. This effect will reduce the light intensity, which is expected to be the relevant quantitative parameter determining efficacy of ChR2 stimulation. We therefore next calculated the effective intensity, taking into account the combined effects of scattering, absorption and conical spread (figure 3(c)). The relationship of intensity to tissue penetration distance was estimated by taking the product of the measured transmission fraction (total remaining light not scattered or absorbed) and the calculated fractional decrease in intensity due to the conical geometry of emitted light at a given distance in the absence of tissue scattering and absorption (methods).

Together, these experimental observations and calculations (figure 3(c)) allowed us to estimate the expected volume of tissue activated by this implementation of the optical neural interface. If effective ChR2-induced spiking is achieved at 1 mW mm^{-2}, then with the current laser diode and fiberoptic technology the optical neural interface in principle will be capable of evoking spiking in neurons at least up to 1.4 mm from the fiber tip. This distance value, together with the measured conical cross-section of 1 mm diameter at 1.4 mm from the fiber tip, results in a total volume experiencing $\geqslant$1 mW mm^{-2} light intensity of ∼0.5 mm^3. This volume represents a substantial volume of brain tissue on the same order of magnitude as features on the somatotopic maps on motor cortex, and indicated to us that the optical design of the neural interface, in combination with the previously tested genetic design, could suffice to drive motor cortex function in the intact animal.

3.4. Optical control of motor output

We next tested whether the optical neural interface could be used to control motor output. Having demonstrated that functional ChR2 can be expressed in the deeper layers of vibrissal motor cortex, we hypothesized that activation of these neurons using the optical neural interface would cause detectable whisker movements. Previous work has shown that electrical stimulation of vibrissal motor cortex results in whisker deflections [39, 40], and that firing of even a single layer 5 or 6 motor neuron will evoke deflections [48].

To quantify whisker deflection, we attached a magnetic particle to the C2 whisker and tracked its movement using a magnetic field sensor (figure 4(a)) [44]. We found that indeed pulsed blue light delivered via the optical neural interface

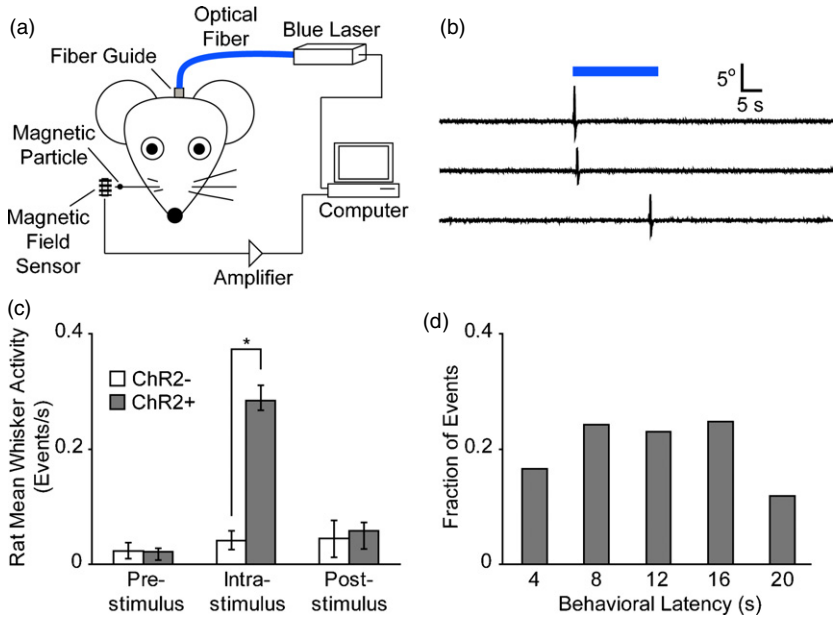

Figure 4. Optical control of motor output in rat. (a) Schematic of whisker movement measurement setup. Top: optical neural interface used to activate rat vibrissal motor cortex: the blue laser diode was coupled to a 200 μm multimode silica-core optical fiber. The fiber was directed at the motor cortex using the implanted fiber guide. Blue light (473 nm) was transmitted to the vibrissal motor cortex via the optical fiber. Whisker movements were measured magnetically (methods); a magnetic particle was attached to the contralateral C2 vibrissa and a magnetoresistive sensor was placed near the particle. Changes in the voltage were amplified electronically and recorded to a computer. The signal was high-pass filtered at 10 Hz to remove low-frequency drift. (b) Whisker activity in a ChR2+ rat in response to a 20 s continuous pulse of blue light. Three consecutive sweeps are shown. Scale bars: 5° and 5 s. (c) Rat mean whisker activity pre-stimulus, intra-stimulus and post-stimulus. The mean number of whisker twitching events was significantly greater in the ChR2+ rats (lentivirus injected through the fiber guide, $n = 2$) than in the ChR2− rats (vehicle injected through fiber guide, $n = 2$), $^*p < 0.05$. (d) Histogram of behavioral latency; time from stimulus onset to whisker deflection; 4 s bins; all events included.

repeatedly evoked whisker deflections in the rat (figure 4(b)) of up to 10°. The mean number of whisker deflection events during stimulation was significantly higher in the ChR2+ rats than in the ChR2– control rats ($p < 0.05$) (figure 4(c)). The control rats had an ONI implanted, but received a vehicle injection through the fiber guide in lieu of the virus. The lack of increase in whisker activity during stimulation in the control rats indicates that the evoked activity was directly due to ChR2 activation and not due to a non-ChR2 effect related to the light delivery, such as a startle response or local nonspecific tissue effects of light delivery. Individual whisker deflection events occurred throughout the duration of the stimulus (figure 4(d)). The successful generation of a motor output indicates that ChR2 under control of the ONI is not only able to optically stimulate targeted cells but also to trans-synaptically recruit downstream neurons [21] (e.g. thalamic and cranial nerve neurons) in the motor pathway leading to muscle contraction.

The laboratory rat is a widely used animal model for many neurological and psychiatric diseases relevant to brain stimulation work. However, mice are the ideal animal model for studying genetic contributions to nervous system physiology and pathology, despite the fact that mice can be more challenging for neural interface work due to their much smaller size. Therefore, the optical neural interfaces were also implanted and tested in mice. As in the rat, 20 s blue light pulses delivered with the ONI evoked whisker deflections (figure 5(a)) up to 20°. Again, the mean number of deflections during the stimulus period was significantly higher in the ChR2+ mice than in the ChR2– mice ($p < 0.05$) (figure 5(b)). The amplitude of the whisker deflections was also analyzed, and demonstrated an increase in the amplitude of whisker deflection during the stimulus period when compared with the pre-stimulus period ($p < 0.05$) (figure 5(c)). Latencies to behavioral output (figure 5(d)) were similar to those observed in the rat and presumably reflect complexities of motor circuit function *in vivo*; these data are consistent with the interpretation that optogenetic activation of this population of cells in motor cortex stably increases the probability of triggering functional motor output during the period of illumination. Together, these data demonstrate successful implementation of an optical neural interface.

3.5. Neuron type-specific activation via optical stimulation

Finally, we sought to confirm that we were indeed stimulating a select genetically defined set of neurons via this integrated optical and genetic technology. We employed immunohistochemistry to verify that ChR2 was expressed specifically in the excitatory cortical pyramidal neurons (figure 6), as hypothesized from our use of the glutamatergic, neuron-specific, CaMKIIα promoter to drive ChR2 expression. Fixed brain sections of injected animals were immunostained as floating sections with an antibody for dsRed to label ChR2-mCherry, along with antibodies for either CaMKIIα or glutamate decarboxylase (GAD67),

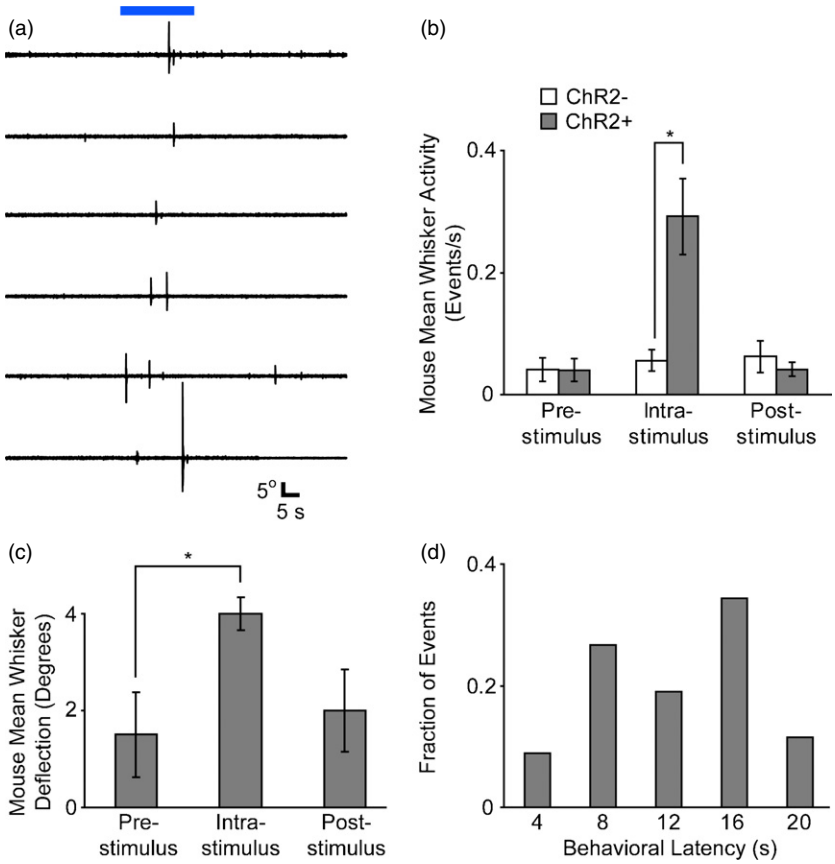

Figure 5. Optical control of motor output in mouse. (a) Whisker activity in a ChR2+ mouse in response to a 20 s pulse of blue light. Six consecutive sweeps are shown. (b) Mouse mean whisker activity pre-stimulus, intra-stimulus, and post-stimulus. ChR2+ mice (lentivirus injected through the fiber guide, $n = 4$) had significantly more whisker twitching events than ChR2− mice (vehicle injected through fiber guide, $n = 3$), $^{*}p < 0.05$. Comparisons of whisker activity pre-stimulus and post-stimulus were not significantly different in either the ChR2– or ChR2+ mice, both $p > 0.5$. (c) Mouse mean whisker deflection amplitude pre-stimulus, intra-stimulus, and post-stimulus. Deflection amplitude was significantly larger during the light pulse, $^{*}p < 0.05$. (d) Histogram of behavioral latency; time from stimulus onset to whisker deflection; 4 s bins; all events included.

a GABA-producing enzyme that is specifically expressed in inhibitory interneurons. Representative confocal images of ChR2/CaMKIIα and ChR2/GAD67 immunostaining are shown (figure 6). We observed that 95% of the ChR2-positive cells in the cortex also expressed CaMKIIα (illustrated in figures 6(a)–(c)), and 0% expressed GAD67 (illustrated in figures 6(d)–(f)). Thus, ChR2 expression was specific to the excitatory CaMKIIα-expressing cortical neuron population. As a consequence, the optical neural interface selectively activates excitatory cortical neurons and not other cell types such as inhibitory neurons or glial cells, a key advantage of this interface design.

4. Discussion

4.1. Summary of results

In this paper we present results showing the successful development and implementation of a novel optical neural interface based on integrated fiberoptic and optogenetic technology [21]. This interface employs an implanted fiber guide to target the brain region of interest (vibrissal motor cortex in this case). This fiber guide was used to (1) deliver the engineered viruses that render specific neuronal types optically sensitive through ChR2 expression and (2) direct the illumination beam of the optical fiber to the ChR2+ neurons. Using this interface, optical control of the rodent's motor system was achieved. Indeed, robust, high-amplitude whisker deflections were evoked when blue light was delivered by the optical neural interface. The interface was implemented in both a rat and a mouse model, and was verified to target specific neuronal cell types.

4.2. Comparison with other methods

Traditionally, electrodes have been the most valuable tool for stimulating neurons, both in the laboratory and in the setting of clinical neuromodulation. Electrodes can 'speak the language' of neurons, approximating natural excitatory cellular signals on the millisecond timescale. While large myelinated axons may be preferentially activated [49–52], electrodes are largely agnostic with regard to the type of the neurons that they stimulate. Consequently, physical proximity of an electrode pole to the neuron may be the single largest determining factor with regard to which neurons will be stimulated. Accordingly, it is generally not feasible to restrict stimulation absolutely

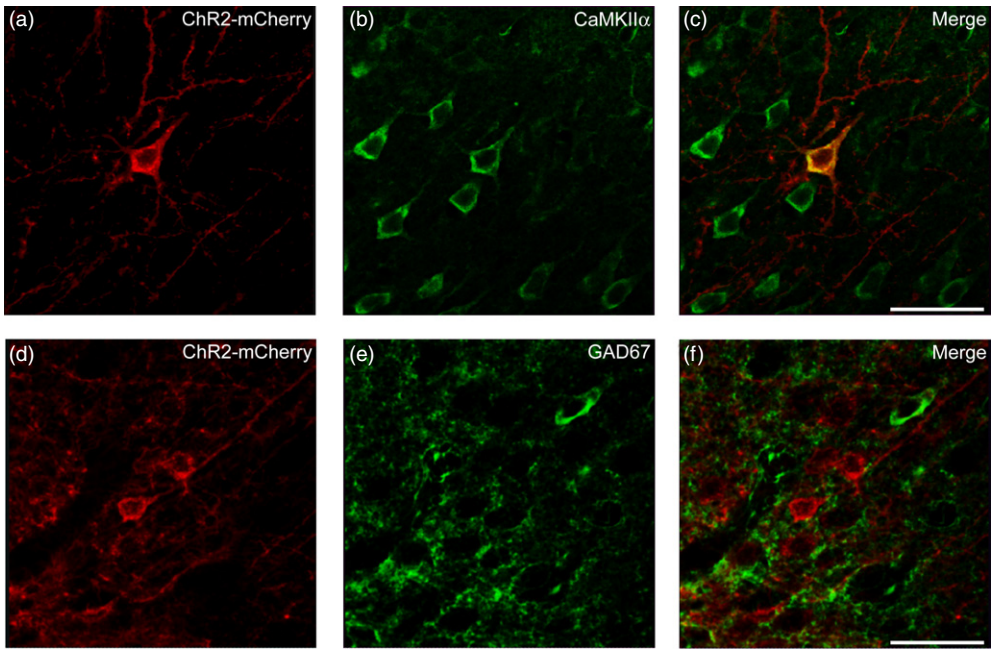

Figure 6. ChR2 expression is specific to excitatory glutamatergic neurons. (a), (d) Cortical sections of mouse brains infected with lentiviruses carrying the ChR2-mCherry fusion protein under the CaMKIIα promoter were immunostained for mCherry. (b) Same section in (a) immunostained for the excitatory glutamatergic neuronal marker CaMKIIα. (c) Merged image of (a), (b) showing colocalization between ChR2-mCherry and CamKIIα. (e) Same section as (d) immunostained for the inhibitory GABAergic neuronal marker GAD67. (f) Merged image of (d), (f) showing no colocalization of ChR2-mCherry with GAD67. Scale bar is 50 μm.

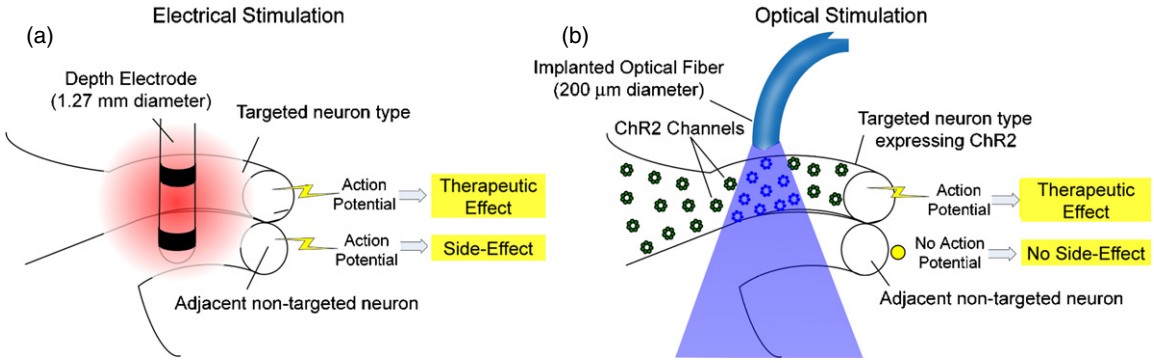

Figure 7. Comparing effects of electrical and optogenetic stimulation of neural tissue. (a) Electrical stimulation non-specifically affects all cell types near the electrode. (b) By contrast, optogenetic stimulation affects only those neurons of a specific type that have been genetically targeted to express ChR2. Schematic not to scale.

to a single class of neuron, in contrast to the level of control afforded by the optical neural interface technology described here.

With electrode-based deep brain stimulation (DBS), the distinctions among treatment efficacy failure, stimulation-induced side effects and even successful therapeutic effects are sometimes unclear. For example, does the eventual rebound of tremor and rigidity in a Parkinson's patient implanted with a DBS electrode result from electrode failure, peri-electrode glial scarring or neurophysiological adaptation of the targeted neurons? Alternatively, might the rebound of symptoms be inevitable even with ongoing successful stimulation of the target neurons, resulting instead from chronic stimulation of a non-targeted neuron population resulting in a gradually acquired functional adaptation? Similarly, are the promising effects of DBS to brain area Cg25 in patients with chronic depression attributable to direct inhibition of Cg25 [15], or might electrical spillover of a magnitude sufficient to cause effects in the basal ganglia be separately inducing therapeutic activity elsewhere? Such questions remain compelling areas for future investigation, now perhaps more accessible with the advent of optogenetic control [21], with greater spatial precision sufficient to permit the selective control of distinct cell types in specific neural circuits (figure 7). Even in cases where non-specific stimulation could be desirable, gaining knowledge of which cell types are responsible for therapeutic success or failure is crucial to furthering our understanding of these neuromodulation therapies.

Additional problematic features of electrode stimulation could become less significant with the optical interface. For example, on the timescale of months, deep brain stimulation (DBS) electrode-leads frequently become encapsulated by

Table 1. Comparison of neuromodulation modalities (electrical, magnetic, and optogenetic).

	Electrical	Magnetic	Optogenetic
Implantation	Electrode and wire	Not necessary	Light source and gene
Spatial precision	Moderate (mm)	Low (cm)	High (single cell)
Neural depolarization	Yes	Yes	Yes
Neural hyperpolarization	Not readily	Not readily	Yes (direct inhibition)
Cell-type specificity	Low	Low	High
Temporal precision	High (ms)	High (ms)	High (ms)

glial cells [53], elevating the electrical impedance and therefore the electrical power delivery required to reach targeted cells. However, compensatory increases in voltage, frequency or pulse width to increase spread of electrical current may increase unintended stimulation of non-target cell populations, with the emergence of side effects [52, 54, 55]. Glia are effective electrical insulators, but are also largely optically transparent, and therefore the optical neural interface has the potential to serve as a much more stable long-term interface technology in the setting of inevitable glial scar formation. The movement of the brain relative to the skull is another potential source of local tissue damage if the optics are hard-anchored to the skull [56, 57]. Such problems may be overcome through the use of optoelectronic elements implanted within the brain tissue. Additional long-term experimental work, tracking implant efficacy on the timescale of many months to years, will be needed to test this hypothesis.

Another method of brain stimulation is transcranial magnetic stimulation (TMS), which is emerging as a safe and effective treatment for conditions including depression, tinnitus and trigeminal neuralgia. In this method, large magnetic fields (>1 T) are generated by custom coils apposed to the head carrying large currents (up to 8000 A) in very brief pulses (<1 ms); the resulting rapidly changing magnetic fields cross the scalp and skull without significant pain or discomfort and induce electrical currents in cortical brain tissue. While appealing because of its noninvasive character, TMS is limited by rapid fall off of power with distance from the surface of the coil [58–60] and cannot, at present, achieve focus at depth [61, 62]. Consequently, only surface cortical structures can be directly stimulated in a spatially focused manner. This contrasts with implantable electrical and optical neural interfaces, both of which can target arbitrarily deep structures. Additionally, enormous currents and large amounts of electrical energy are required due to the inefficient inductive conversion process, and finally, like electrodes, TMS is of course generally agnostic with respect to the type of neurons activated.

4.3. Challenges and future directions in development of the optical neural interface

Potential challenges relating to the ONI include the fact that the gene must be introduced into the target tissue, and that the volume of tissue activated is currently limited by the light intensity delivered through the fiber. Regarding the genetic aspect, gene therapy in neurons (nonproliferative cells that are non-susceptible to neoplasms) is proceeding rapidly, with active, FDA-approved clinical trials already underway involving viral gene delivery to human brains (www.ceregene.com). Moreover, the utility of this technology extends far beyond direct clinical applications. First, important clinical utility will result from application of this method to animal models of DBS, for example in Parkinsonian rats [63–65], to identify the target cell types responsible for therapeutic effects (an area of intense debate and immense clinical importance [13, 66]). This knowledge alone may lead to the development of improved pharmacological and surgical strategies for treating human disease. Second, for basic neuroscience investigations, this method appears powerful enough to link genetically defined cell types with complex systems-level behaviors, and may allow the elucidation of the precise contribution of different cell types in many different brain regions to high-level organismal functioning.

Regarding volume of tissue activated, while the volumes activated with this technology sufficed to control systems level functioning in the work presented here, larger volumes of activation could be important in other settings, for example in large-scale neural prosthetic applications. However, our measurements and calculations very likely give rise to a lower limit on volume of tissue activatable with the ONI. Neurons at higher physiological temperatures will be more excitable than those in our *in vitro* experiments in which light power requirements were quantitatively measured. Moreover, our optical fiber is several-fold thinner than the diameter of current DBS electrodes (1.27 mm, www.medtronic.com), and enlarging the fiber will markedly enlarge the volume of tissue activated (20 mm^3 for a 1 mm diameter optical fiber).

The ONI described in this paper provides a method for increasing neural activity. While useful for many applications, direct neural inhibition may be more appropriate for others. Toward this end, our lab and others have developed optogenetic techniques for suppressing neural activity in intact living neural circuits; a vertebrate rhodopsin has been shown to inhibit neural activity in chick spinal cord [32], and we recently have demonstrated that a specific halorhodopsin from Natronomonas pharaonis (NpHR, a light-activated chloride pump) can be used to suppress neural activity, in slices of intact mammalian neural tissue, with high temporal precision [67]. It has also been suggested from work in cell culture that this method could be used to desynchronize or inhibit neurons [68]. This approach opens up the possibility of making inhibitory ONIs for intact mammalian brain tissue; the ability to 'turn off' neurons *in vivo* in a fast reversible manner will likely be useful in both basic and clinical neuroscience.

In summary, this combined optical and genetic (optogenetic [21]) neural interface design offers several

possible advantages over electrical and magnetic techniques (table 1). First, the ONI provides a privileged channel of communication that does not affect non-targeted cell populations. Second, the ONI will likely be less susceptible to signal attenuation due to gliosis. Third, the diffuse light scattering and gradual, acute-angle beam divergence from the depth-targeted optical fiber source give rise to a suitable depth penetration profile. The ONI also conserves important features of electrical and magnetic stimulation, including millisecond-scale temporal precision. Finally, the hardware involved with the ONI is not significantly more bulky than current DBS hardware, and the long, flexible, lightweight optical fiber method separates resistive heat-generating elements from the target tissue.

5. Conclusion

Optical neuromodulation remains in the early stages of research, but offers a number of promising technological advantages. While a great deal of engineering and technology development remain to be conducted, the optical neural interface raises the prospect of specific interventions such as controlling motor fibers while leaving immediately adjacent pain fibers undisturbed (or vice versa), and selectively controlling excitatory or inhibitory neurons in DBS target regions. On the basic science side, ChR2-expressing animals have been useful for fast and precisely targeted electrophysiological circuit mapping [69–71]. The optical neural interface mediating behavior in intact animals described here now pushes optogenetic technology beyond electrophysiological studies to determining the causal role of specific cell types in complex animal behaviors. Targeted, temporally precise control of specific neuronal subtypes may lead to insights into clinically relevant neuromodulation with fewer side effects and more robust therapeutic efficacy, as well as insights into the cellular basis of systems-level neural circuit function.

Acknowledgments

AA is supported by a fellowship from the Walter V and Idun Berry Foundation, LW is supported by a fellowship from the California Institute of Regenerative Medicine, FZ is supported by a fellowship from the NIH, LM and MM are supported by fellowships from Stanford Bio-X, and MBS is supported by the Coulter Foundation. We thank Michael Brecht (University Medical Center Rotterdam) and Rune Berg (University of Copenhagen) for technical advice on surgical procedures and the magnetic whisker assay. KD is supported by NIMH, NIDA and NIGMS, as well as by NARSAD, APIRE and the Snyder, Culpeper, Coulter, Klingenstein, Whitehall, McKnight, and Albert Yu and Mary Bechmann Foundations.

References

[1] Donoghue J P, Nurmikko A, Black M and Hochberg L 2007 Assistive technology and robotic control using MI ensemble-based neural interface systems in humans with tetraplegia *J. Physiol.* **579** 603–11

[2] Middlebrooks J C, Bierer J A and Snyder R L 2005 Cochlear implants: the view from the brain *Curr. Opin. Neurobiol.* **15** 488–93

[3] Shepherd R K and McCreery D B 2006 Basis of electrical stimulation of the cochlea and the cochlear nucleus *Adv. Otorhinolaryngol.* **64** 186–205

[4] Lertmanorat Z and Durand D M 2004 A novel electrode array for diameter-dependent control of axonal excitability: a simulation study *IEEE Trans. Biomed. Eng.* **51** 1242–50

[5] Stein R B and Mushahwar V 2005 Reanimating limbs after injury or disease *Trends Neurosci.* **28** 518–24

[6] Talwar S K, Xu S, Hawley E S, Weiss S A, Moxon K A and Chapin J K 2002 Rat navigation guided by remote control *Nature* **417** 37–8

[7] Pesaran B, Musallam S and Andersen R A 2006 Cognitive neural prosthetics *Curr. Biol.* **16** R77–80

[8] Jackson A, Moritz C T, Mavoori J, Lucas T H and Fetz E E 2006 The Neurochip BCI: towards a neural prosthesis for upper limb function *IEEE Trans. Neural. Syst. Rehabil. Eng.* **14** 187–90

[9] Kirsch R F, Acosta A M, van der Helm F C, Rotteveel R J and Cash L A 2001 Model-based development of neuroprostheses for restoring proximal arm function *J. Rehabil. Res. Dev.* **38** 619–26

[10] Pancrazio J J, Kulagina N V, Shaffer K M, Gray S A and O'Shaughnessy T J 2004 Sensitivity of the neuronal network biosensor to environmental threats *J. Toxicol. Environ. Health* A **67** 809–18

[11] Bevan M D, Atherton J F and Baufreton J 2006 Cellular principles underlying normal and pathological activity in the subthalamic nucleus *Curr. Opin. Neurobiol.* **16** 621–8

[12] Grill W M 2005 Safety considerations for deep brain stimulation: review and analysis *Expert Rev. Med. Dev.* **2** 409–20

[13] McIntyre C C, Savasta M, Walter B L and Vitek J L 2004 How does deep brain stimulation work? Present understanding and future questions *J. Clin. Neurophysiol.* **21** 40–50

[14] Perlmutter J S and Mink J W 2006 Deep brain stimulation *Annu. Rev. Neurosci.* **29** 229–57

[15] Mayberg H S, Lozano A M, Voon V, McNeely H E, Seminowicz D, Hamani C, Schwalb J M and Kennedy S H 2005 Deep brain stimulation for treatment-resistant depression *Neuron* **45** 651–60

[16] Mandat T S, Hurwitz T and Honey C R 2006 Hypomania as an adverse effect of subthalamic nucleus stimulation: report of two cases *Acta Neurochir. (Wien)* **148** 895–7; discussion 898

[17] Blomstedt P and Hariz M I 2006 Are complications less common in deep brain stimulation than in ablative procedures for movement disorders *Stereotact. Funct. Neurosurg.* **84** 72–81

[18] Hariz M I 2002 Complications of deep brain stimulation surgery *Mov. Disord.* **17** (suppl 3) S162–6

[19] Deuschl G *et al* 2006 Deep brain stimulation: postoperative issues *Mov. Disord.* **21** (suppl 14) S219–37

[20] Greenberg B D and Rezai A R 2003 Mechanisms and the current state of deep brain stimulation in neuropsychiatry *CNS Spectr.* **8** 522–6

[21] Deisseroth K, Feng G, Majewska A K, Miesenbock G, Ting A and Schnitzer M J 2006 Next-generation optical technologies for illuminating genetically targeted brain circuits *J. Neurosci.* **26** 10380–6

[22] Zhang F, Wang L P, Boyden E S and Deisseroth K 2006 Channelrhodopsin-2 and optical control of excitable cells *Nat. Methods* **3** 785–92

[23] Miesenbock G and Kevrekidis I G 2005 Optical imaging and control of genetically designated neurons in functioning circuits *Annu. Rev. Neurosci.* **28** 533–63

[24] Kramer R H, Chambers J J and Trauner D 2005 Photochemical tools for remote control of ion channels in excitable cells *Nat. Chem. Biol.* **1** 360–5

[25] Callaway E M and Katz L C 1993 Photostimulation using caged glutamate reveals functional circuitry in living brain slices *Proc. Natl Acad. Sci. USA* **90** 7661–5

[26] Zemelman B V, Nesnas N, Lee G A and Miesenbock G 2003 Photochemical gating of heterologous ion channels: remote control over genetically designated populations of neurons *Proc. Natl Acad. Sci. USA* **100** 1352–7

[27] Melyan Z, Tarttelin E E, Bellingham J, Lucas R J and Hankins M W 2005 Addition of human melanopsin renders mammalian cells photoresponsive *Nature* **433** 741–5

[28] Banghart M, Borges K, Isacoff E, Trauner D and Kramer R H 2004 Light-activated ion channels for remote control of neuronal firing *Nat. Neurosci.* **7** 1381–6

[29] Volgraf M, Gorostiza P, Numano R, Kramer R H, Isacoff E Y and Trauner D 2006 Allosteric control of an ionotropic glutamate receptor with an optical switch *Nat. Chem. Biol.* **2** 47–52

[30] Boyden E S, Zhang F, Bamberg E, Nagel G and Deisseroth K 2005 Millisecond-timescale, genetically targeted optical control of neural activity *Nat. Neurosci.* **8** 1263–8

[31] Ishizuka T, Kakuda M, Araki R and Yawo H 2006 Kinetic evaluation of photosensitivity in genetically engineered neurons expressing green algae light-gated channels *Neurosci. Res.* **54** 85–94

[32] Li X, Gutierrez D V, Hanson M G, Han J, Mark M D, Chiel H, Hegemann P, Landmesser L T and Herlitze S 2005 Fast noninvasive activation and inhibition of neural and network activity by vertebrate rhodopsin and green algae channelrhodopsin *Proc. Natl Acad. Sci. USA* **102** 17816–21

[33] Nagel G, Brauner M, Liewald J F, Adeishvili N, Bamberg E and Gottschalk A 2005 Light activation of channelrhodopsin-2 in excitable cells of Caenorhabditis elegans triggers rapid behavioral responses *Curr. Biol.* **15** 2279–84

[34] Nagel G, Ollig D, Fuhrmann M, Kateriya S, Musti A M, Bamberg E and Hegemann P 2002 Channelrhodopsin-1: a light-gated proton channel in green algae *Science* **296** 2395–8

[35] Nagel G, Szellas T, Huhn W, Kateriya S, Adeishvili N, Berthold P, Ollig D, Hegemann P and Bamberg E 2003 Channelrhodopsin-2, a directly light-gated cation-selective membrane channel *Proc. Natl Acad. Sci. USA* **100** 13940–5

[36] Zemelman B V, Lee G A, Ng M and Miesenbock G 2002 Selective photostimulation of genetically ChARGed neurons *Neuron* **33** 15–22

[37] Zhang Y P and Oertner T G 2007 Optical induction of synaptic plasticity using a light-sensitive channel *Nat. Methods* **4** 139–41

[38] Bi A, Cui J, Ma Y P, Olshevskaya E, Pu M, Dizhoor A M and Pan Z H 2006 Ectopic expression of a microbial-type rhodopsin restores visual responses in mice with photoreceptor degeneration *Neuron* **50** 23–33

[39] Berg R W and Kleinfeld D 2003 Vibrissa movement elicited by rhythmic electrical microstimulation to motor cortex in the aroused rat mimics exploratory whisking *J. Neurophysiol.* **90** 2950–63

[40] Kleinfeld D, Berg R W and O'Connor S M 1999 Anatomical loops and their electrical dynamics in relation to whisking by rat *Somatosens. Mot. Res.* **16** 69–88

[41] Vo-Dinh T 2003 *Biomedical Photonics Handbook* (Boca Raton, FL: CRC Press)

[42] Bevilacqua F, Piguet D, Marquet P, Gross J D, Tromberg B J and Depeursinge C 1999 In vivo local determination of tissue optical properties: applications to human brain *Appl. Opt.* **38** 4939–50

[43] Yaroslavsky A N, Schulze P C, Yaroslavsky I V, Schober R, Ulrich F and Schwarzmaier H J 2002 Optical properties of selected native and coagulated human brain tissues in vitro in the visible and near infrared spectral range *Phys. Med. Biol.* **47** 2059–73

[44] Berg R W and Kleinfeld D 2003 Rhythmic whisking by rat: retraction as well as protraction of the vibrissae is under active muscular control *J. Neurophysiol.* **89** 104–17

[45] Svoboda K and Yasuda R 2006 Principles of two-photon excitation microscopy and its applications to neuroscience *Neuron* **50** 823–39

[46] Liu X B and Jones E G 1996 Localization of alpha type II calcium calmodulin-dependent protein kinase at glutamatergic but not gamma-aminobutyric acid (GABAergic) synapses in thalamus and cerebral cortex *Proc. Natl Acad. Sci. USA* **93** 7332–6

[47] Tighilet B, Huntsman M M, Hashikawa T, Murray K D, Isackson P J and Jones E G 1998 Cell-specific expression of type II calcium/calmodulin-dependent protein kinase isoforms and glutamate receptors in normal and visually deprived lateral geniculate nucleus of monkeys *J. Comp. Neurol.* **390** 278–96

[48] Brecht M, Schneider M, Sakmann B and Margrie T W 2004 Whisker movements evoked by stimulation of single pyramidal cells in rat motor cortex *Nature* **427** 704–10

[49] Nowak L G and Bullier J 1998 Axons, but not cell bodies, are activated by electrical stimulation in cortical gray matter. II. Evidence from selective inactivation of cell bodies and axon initial segments *Exp. Brain Res.* **118** 489–500

[50] Nowak L G and Bullier J 1998 Axons, but not cell bodies, are activated by electrical stimulation in cortical gray matter: I. Evidence from chronaxie measurements *Exp. Brain Res.* **118** 477–88

[51] Ranck J B Jr 1975 Which elements are excited in electrical stimulation of mammalian central nervous system: a review *Brain Res.* **98** 417–40

[52] Volkmann J, Herzog J, Kopper F and Deuschl G 2002 Introduction to the programming of deep brain stimulators *Mov. Disord.* **17** (suppl. 3) S181–7

[53] Polikov V S, Tresco P A and Reichert W M 2005 Response of brain tissue to chronically implanted neural electrodes *J. Neurosci. Methods* **148** 1–18

[54] Montgomery E B Jr 2004 Deep brain stimulation for hyperkinetic disorders *Neurosurg. Focus* **17** E1

[55] Butson C R and McIntyre C C 2005 Tissue and electrode capacitance reduce neural activation volumes during deep brain stimulation *Clin. Neurophysiol.* **116** 2490–500

[56] Gilletti A and Muthuswamy J 2006 Brain micromotion around implants in the rodent somatosensory cortex *J. Neural Eng.* **3** 189–95

[57] Lee H, Bellamkonda R V, Sun W and Levenston M E 2005 Biomechanical analysis of silicon microelectrode-induced strain in the brain *J. Neural Eng.* **2** 81–9

[58] Epstein C M, Verson R and Zangaladze A 1996 Magnetic coil suppression of visual perception at an extracalcarine site *J. Clin. Neurophysiol.* **13** 247–52

[59] Maccabee P J, Eberle L, Amassian V E, Cracco R Q, Rudell A and Jayachandra M 1990 Spatial distribution of the electric field induced in volume by round and figure '8' magnetic coils: relevance to activation of sensory nerve fibers *Electroencephalogr. Clin. Neurophysiol.* **76** 131–41

[60] Zangen A, Roth Y, Voller B and Hallett M 2005 Transcranial magnetic stimulation of deep brain regions: evidence for efficacy of the H-coil *Clin. Neurophysiol.* **116** 775–9

[61] Roth Y, Amir A, Levkovitz Y and Zangen A 2007 Three-dimensional distribution of the electric field induced in the brain by transcranial magnetic stimulation using figure-8 and deep H-coils *J. Clin. Neurophysiol.* **24** 31–8

[62] Ruohonen J 1998 Transcranial magnetic stimulation: modeling and new techniques *Doctoral Dissertation* Helsinki University of Technology Helsinki, Finland
[63] Schwarting R K and Huston J P 1996 Unilateral 6-hydroxydopamine lesions of meso-striatal dopamine neurons and their physiological sequelae *Prog. Neurobiol.* **49** 215–66
[64] Shi L H, Luo F, Woodward D J and Chang J Y 2006 Basal ganglia neural responses during behaviorally effective deep brain stimulation of the subthalamic nucleus in rats performing a treadmill locomotion test *Synapse* **59** 445–57
[65] Chang J Y, Shi L H, Luo F and Woodward D J 2006 Neural responses in multiple basal ganglia regions following unilateral dopamine depletion in behaving rats performing a treadmill locomotion task *Exp. Brain Res.* **172** 193–207
[66] McIntyre C C, Savasta M, Kerkerian-Le Goff L and Vitek J L 2004 Uncovering the mechanism(s) of action of deep brain stimulation: activation, inhibition, or both *Clin. Neurophysiol.* **115** 1239–48
[67] Zhang F *et al* 2007 Multimodal fast optical interrogation of neural circuitry *Nature* **446** 633–9
[68] Han X and Boyden E S 2007 Multiple-color optical activation, silencing, and desynchronization of neural activity, with single-spike temporal resolution *PLoS One* **2** e299
[69] Wang H J *et al* 2007 High-speed mapping of synaptic connectivity using photostimulation in channelrhodopsin-2 transgenic mice *Proc. Natl Acad. Sci. USA* **104** 8143–8
[70] Arenkiel B R, Peca J, Davison I G, Feliciano C, Deisseroth K, Angustine G J, Ehlers M D and Feng G 2007 *In vivo* light-induced activation of neural circuitry in transgenic mice expressing channelrhodopsin-2 *Neuron* **54** 205–18
[71] Petreanu L, Huber D, Sobczyk A and Svoboda K 2007 Channelrhodopsin-2-assisted circuit mapping of long-range callosal projection *Nat. Neurosci.* **10** 663–8